ACS APPLIED NANO MATERIALS
Cite This: ACS Appl. Nano Mater. XXXX, XXX, XXX−XXX
Article
www.acsanm.org

One-Pot Green Synthesis of Fe_3O_4/MoS_2 0D/2D Nanocomposites and Their Application in Noninvasive Point-of-Care Glucose Diagnostics

Vikas Nandwana,[†,‡] Wenyuan Huang,[†,‡] Yuan Li,[†,‡] and Vinayak P. Dravid*[,†,‡]

[†]Department of Materials Science & Engineering, Northwestern University, Evanston, Illinois 60208, United States
[‡]International Institute of Nanotechnology (IIN), Evanston, Illinois 60208, United States

Supporting Information

ABSTRACT: We report a novel synthesis of Fe_3O_4/MoS_2 zero-dimensional (0D)/two-dimensional (2D) nanocomposites. When bulk MoS_2 is exfoliated in the presence of thiol-functionalized Fe_3O_4 nanoparticles in water, the latter anchor on the exfoliated MoS_2 nanosheets because of thiol affinity toward MoS_2, resulting in the Fe_3O_4/MoS_2 nanocomposites. The one-pot reaction, room temperature processing, and use of aqueous solvents make the synthesis process facile and ecofriendly. Because of the unique 0D/2D morphology, Fe_3O_4/MoS_2 nanocomposites show significantly higher peroxidase-like catalytic activity compared to Fe_3O_4 nanoparticles or MoS_2 nanosheets alone. The enhanced catalytic activity has been used to detect glucose levels down to 2.4 μM in absorbance measurements. Application toward noninvasive point-of-care glucose diagnostics has been explored by developing paper-based "dip and use" test strips that show colorimetric response in the presence of glucose. To achieve this, Fe_3O_4/MoS_2 nanocomposites along with other active sensing elements are printed onto paper via a desktop inkjet printer and cut into strips. When dipped into solutions of various glucose concentrations, the test strips allow colorimetric detection of glucose concentrations in a qualitative and quantitative manner. To demonstrate practical usage, we have shown that the Fe_3O_4/MoS_2 nanocomposite-based glucose test strips are sufficient to distinguish between normal (healthy) and higher (diabetic) glucose concentrations with the naked eye. Because of the simple and ecofriendly preparation and sensing efficacy with low limit of detection, Fe_3O_4/MoS_2 nanocomposites show promise in noninvasive point-of-care medical diagnostics.

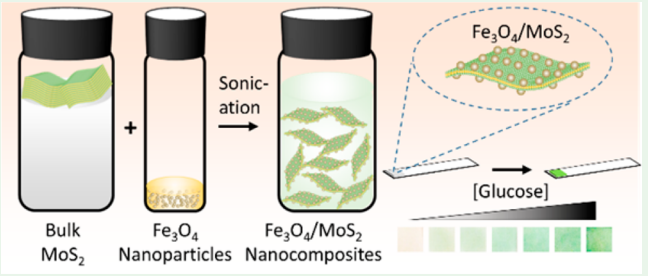

KEYWORDS: *0D/2D nanocomposites, peroxidase mimic, point-of-care diagnostics, biosensing, glucose detection, paper-based sensors, green synthesis*

INTRODUCTION

Over the past few years, transition-metal dichalcogenides have drawn tremendous interest as two-dimensional (2D) nanomaterials beyond graphene.[1−5] In particular, MoS_2 has found a special place because of its unique optical and electronic properties.[6] It has been shown that, as a host matrix, MoS_2 nanosheets can be integrated with a variety of inorganic nanoparticles to develop zero-dimensional (0D)/2D nanocomposites.[7−18] Among various inorganic nanoparticles, Fe_3O_4 nanoparticles have received a lot of attention because of their biocompatibility, stability, superparamagnetic nature, and theranostic properties.[19−26] Therefore, the integration of MoS_2 and Fe_3O_4 has recently become a topic of interest. Fe_3O_4/MoS_2 nanocomposites have shown novel or enhanced functionalities over their individual components alone, leading to their use in environmental, biomedical, energy storage, catalysis, and spintronic applications.[12−18] However, in all of the previously reported syntheses of Fe_3O_4/MoS_2 nanocomposites, first MoS_2 nanosheets were synthesized/exfoliated and then Fe_3O_4 nanoparticles were decorated/grown onto their surface. These methods involve multiple steps, organic solvents, and high processing pressures/temperatures, limiting their use in industrial-scale applications.

On the basis of this motivation, we report a one-pot facile and green synthesis of 0D/2D nanocomposites by attaching 0D nanoparticles during the exfoliation of 2D materials. Fe_3O_4/MoS_2 nanocomposites have been obtained by simply sonicating bulk MoS_2 powder and thiol-functionalized Fe_3O_4 nanoparticles in water (Scheme 1). When bulk MoS_2 exfoliates during sonication, Fe_3O_4 nanoparticles anchor onto the freshly exfoliated MoS_2 nanosheets' surface because of the terminated thiol group's affinity toward surface defects onto MoS_2.[27−30] Apart from providing unique functional properties, thiol-functionalized Fe_3O_4 nanoparticles work as stabilizers and allow the stable dispersion of MoS_2 nanosheets in water. The room temperature processing and use of water makes this method more facile and ecofriendly than previously reported liquid exfoliation processes that involve organic solvents, ion intercalation, and/or higher pressures and temperatures.[31−33]

Received: March 16, 2018
Accepted: March 26, 2018
Published: March 26, 2018

ACS Publications © XXXX American Chemical Society

DOI: 10.1021/acsanm.8b00429
ACS Appl. Nano Mater. XXXX, XXX, XXX−XXX

Scheme 1. Synthesis of Fe_3O_4/MoS_2 Nanocomposites via Thiol-Functionalized Fe_3O_4 Nanoparticle-Assisted Stabilization of Exfoliated MoS_2

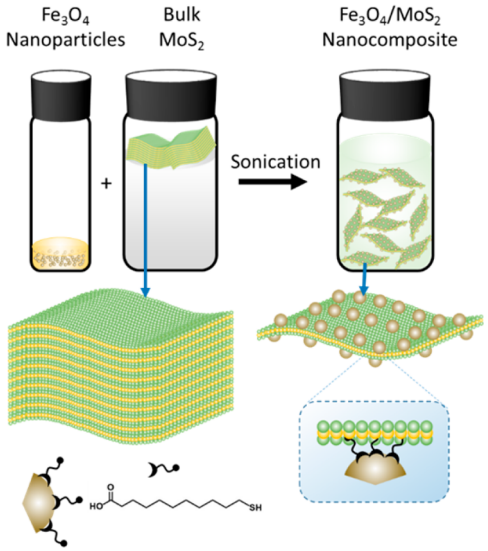

It is reported that 0D/2D nanocomposites show better catalytic ability compared to single-phase counterparts because of the unique 0D/2D morphology.[34,35] Hence, we have explored the peroxidase-like catalytic activity of Fe_3O_4/MoS_2 nanocomposites, which has been demonstrated for a variety of nanomaterials including Fe_3O_4 nanoparticles as well as MoS_2 nanosheets.[24,34−50] We have shown that Fe_3O_4/MoS_2 nanocomposites demonstrate peroxidase-like catalytic activity that is significantly higher than either MoS_2 nanosheets or Fe_3O_4 nanoparticles alone. The enhanced peroxidase activity has been utilized to detect glucose via absorbance measurements with a limit of detection (LOD) equal to 2.4 μM. By inkjet printing Fe_3O_4/MoS_2 nanocomposites and other required sensing elements on paper, test strips are developed that change color in the presence of glucose. When dipped into solutions of various glucose concentrations, the glucose test strips can colorimetrically detect glucose in a dose-dependent manner. The concentration of glucose can also be quantified based on the color of the test strip using a standard calibration curve. Finally, we have shown that paper-based disposable test strips made from Fe_3O_4/MoS_2 nanocomposites can detect glucose concentrations that are sufficient to distinguish glucose levels that are considered normal (health) and higher (diabetic).

EXPERIMENTAL SECTION

Materials. MoS_2 powder, sodium dodecyl sulfate (SDS), 11-mercaptoundecanoic acid (MUA), citric acid, glucose oxidase (GOx), 3,3′,5,5′-tetramethylbenzidine (TMB), *o*-phenylenediamine dihydrochloride (OPD), 2,2′-azinobis(3-ethylbenzothiazoline-6-sulfonic acid) (ABTS), fructose, lactose, and maltose were purchased from Sigma-Aldrich.

Preparation of MoS_2 Nanosheets. MoS_2 nanosheets were prepared using a previously reported aqueous surfactant-assisted exfoliation method.[51] A total of 50 mg of MoS_2 powder, 15 mg of MUA + SDS, and 10 mL of Milli-q water were probe-sonicated for 10 min. MUA and SDS were used to stabilize the MoS_2 nanosheets in water. Then the solution was centrifuged at 4500 rpm for 15 min, and the green supernatant was collected and dialyzed (MWCO = 10000) for 6 h. Any aggregate particles were removed by centrifugation, and finally dispersed MoS_2 nanosheets were stored at room temperature and used as is for further experiments.

Synthesis of Fe_3O_4 Nanoparticles. The Fe_3O_4 nanoparticles were synthesized using previously reported a thermal decomposition method, which resulted in monodispersity and single crystallinity.[20,52] In a typical Fe_3O_4 nanoparticle synthesis, $Fe(acac)_3$ (2 mmol), 1,2-hexadecanediol (10 mmol), oleic acid (6 mmol), oleylamine (6 mmol), and benzyl ether (20 mL) were charged in a 100 mL three-neck, round-bottomed flask and magnetically stirred under a flow of nitrogen. The mixture was first heated to 110 °C for 1 h to remove moisture. Then the temperature was increased to 210 °C for 1 h, and finally the mixture was refluxed for 1 h before cooling to room temperature. The black-brown mixture was precipitated, washed three times using ethanol, and then dispersed in hexane.

Preparation of Thiol-Functionalized Fe_3O_4 Nanoparticles. The as-synthesized oleic acid coated hydrophobic Fe_3O_4 nanoparticles were functionalized with MUA and citric acid via a ligand-exchange process.[20] A chloroform dispersion (2 mL) of Fe_3O_4 nanoparticles (12.5 mg) and a dimethyl sulfoxide (DMSO) solution of MUA (1 mL, 31.25 mg) and CA (1 mL, 31.25 mg) were mixed and sonicated overnight at room temperature under dinitrogen protection. The modified Fe_3O_4 nanoparticles were washed with dichloromethane three times, dried under nitrogen gas, and finally dispersed in water. The dispersion was dialyzed to remove any residual surfactants using a dialysis bag (MWCO = 10000) for 2 days in water. A 200 nm syringe filter was used to remove any precipitation, and the final concentration of thiol-functionalized Fe_3O_4 nanoparticles dispersed in water was determined by inductively coupled plasma mass spectrometry (ICP-MS) analysis. Transmission electron microscopy (TEM) showed that the particles do not aggregate after ligand exchange and hydrodynamic sizes were found in the range of 22−47 nm. The presence of thiol was confirmed by the S peaks in X-ray photoelectron spectroscopy (XPS).

Preparation of Fe_3O_4/MoS_2 Nanocomposites. A total of 50 mg of MoS_2 powder, 0.2 mL of thiol-functionalized Fe_3O_4 nanoparticles ([Fe] = 1 mg/mL), and 10 mL of Milli-q water were probe-sonicated for 10 min. Then the solution was centrifuged at 4500 rpm for 15 min, and the green-brown supernatant was collected and dialyzed using a dialysis bag (MWCO = 10000) for 6 h in water. Any aggregated particles were removed by centrifugation and finally aqueous dispersed Fe_3O_4/MoS_2 nanocomposites were stored at room temperature and used as is for further experiments. The concentration of molybdenum and iron was calculated via ICP-MS. The Fe_3O_4/MoS_2 nanocomposites demonstrate high colloidal stability across a wide pH range (pH 6−10) and at a salt (NaCl) concentration of 50 mM.

Characterization of Fe_3O_4 Nanoparticles, MoS_2 Nanosheets, and Fe_3O_4/MoS_2 Nanocomposites. TEM, energy-dispersive X-ray (EDX), and elemental mapping of the nanostructures were observed by a Hitachi HD2300 instrument. The hydrodynamic diameters of the nanostructures were measured by a Malvern Zeta Sizer Nano S-90 dynamic light scattering instrument. Raman spectra were collected on a Horiba LabRAM HR Evolution Confocal Raman System equipped with a solid-state laser. The laser power used was 8.8 μW with a cocondition of 2. XPS (Thermo Scientific ESCALAB 250Xi) was used for binding energy analysis and elemental confirmation.

Peroxidase Activity of Fe_3O_4/MoS_2 Nanocomposites. The peroxidase-like activity of Fe_3O_4/MoS_2 nanocomposites was tested by mixing 0.2 mL of TMB, 0.2 mL of a Fe_3O_4/MoS_2 dispersion, and 0.2 mL of hydrogen peroxide (H_2O_2) in a 0.1 M citrate phosphate buffer (pH 5.0). The final concentrations of TMB and H_2O_2 were chosen to be 1.25 and 2.5 mM, while the concentrations of Fe_3O_4/MoS_2 were [Mo] = 8 μg/mL and [Fe] = 22 μg/mL. The TMB solution was made in a 0.1 M citrate phosphate buffer (pH 5.0). For ABTS and OPD reaction, a similar method was used. OPD was dissolved in a 0.1 M citrate phosphate buffer (pH 5.0), while ABTS was dissolved in a 0.1 M citrate buffer (pH 5.0). To calculate K_m and V_{max} of Fe_3O_4/MoS_2 using the Michaelis−Menten and Lineweaver−Burk models, steady-state kinetic and double-reciprocal plots were recorded. The velocity (v) of the reaction was measured in a 0.1 M citrate phosphate buffer (pH 5.0) at room temperature. The concentrations of Fe_3O_4/MoS_2 were chosen to be [Mo] = 8 μg/mL and [Fe] = 22 μg/mL. For one set, the concentration of TMB was kept at 1.25 mM and the H_2O_2 concentration was varied. For another set, the concentration of H_2O_2

DOI: 10.1021/acsanm.8b00429
ACS Appl. Nano Mater. XXXX, XXX, XXX−XXX

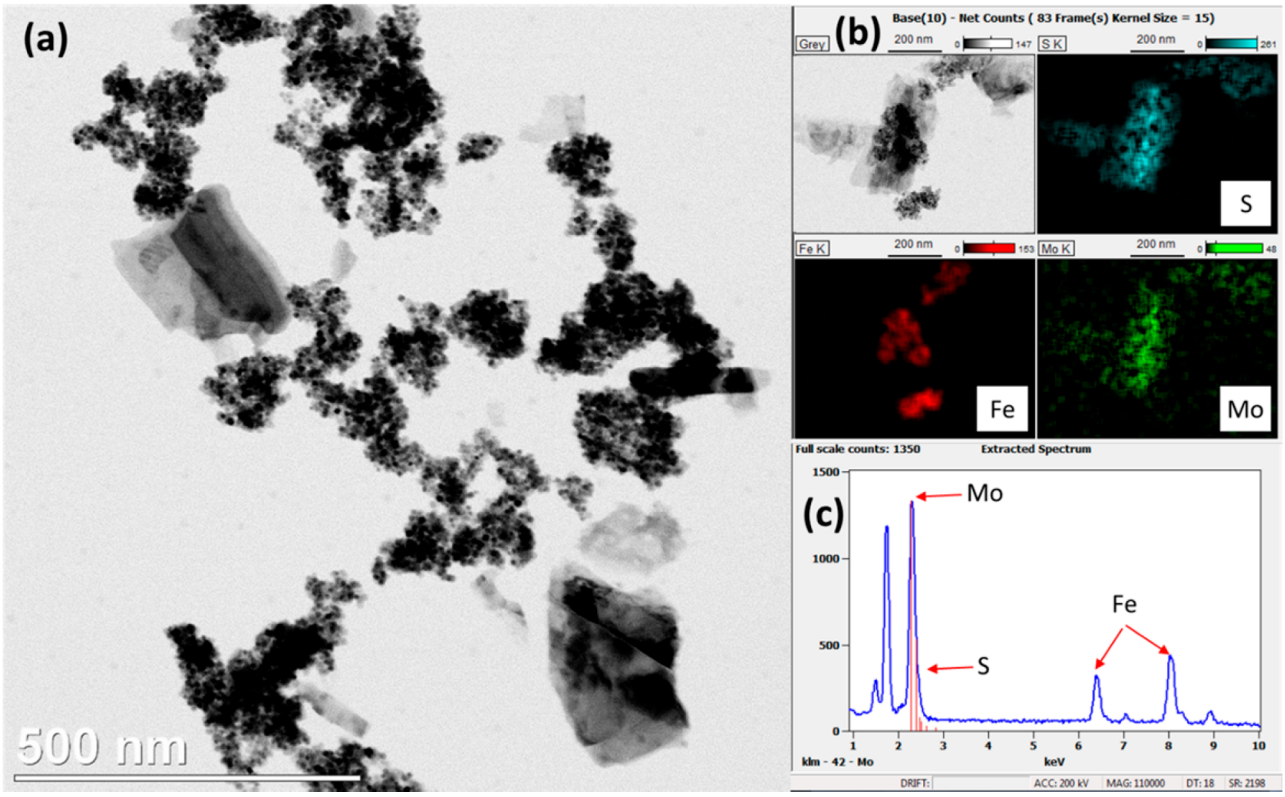

Figure 1. (a) TEM bright-field image, (b) elemental map, and (c) EDX pattern of a Fe_3O_4/MoS_2 nanocomposite. The apparent aggregation could happen during the TEM sample preparation because slow solvent (water in this case) evaporation induces aggregation during drying.

was kept at 2.5 mM and the TMB concentration was varied. Double-reciprocal plots of the catalytic activity of Fe_3O_4/MoS_2 had a fixed concentration of one substrate (H_2O_2 or TMB) while the other was varied.

Detection of H_2O_2 and Glucose in Solution. For H_2O_2 detection, first 0.2 mL of TMB in a pH 5.0 citrate phosphate buffer and 0.2 mL of Fe_3O_4/MoS_2 were mixed. The final concentration of TMB was chosen as 1.25 mM, while the concentrations of Fe_3O_4/MoS_2 were [Mo] = 8 μg/mL and [Fe] = 22 μg/mL. Then, amounts of 0.2 mL of H_2O_2 with different concentrations were added. The reaction rate at 652 nm was recorded immediately after the addition of H_2O_2, while for the absorbance values, the solutions were kept at room temperature for 5 min before recording. The absorbance change was recorded in a BioTek Synergy 4 Multimode plate reader with an onboard dispenser and a monochromator. For glucose detection, a mixture of 0.1 mL of GOx and 0.1 mL of a glucose solution of different concentrations in a 0.1 M Na_2HPO_4 buffer (pH 7.0) was incubated at 37 °C for 30 min. Then, 0.2 mL of TMB in a pH 5.0 citrate phosphate buffer and 0.2 mL of Fe_3O_4/MoS_2 were added. The final concentrations of GOx and TMB were chosen to be 3.33 mg/mL and 1.25 mM, respectively, while concentrations of Fe_3O_4/MoS_2 were [Mo] = 8 μg/mL and [Fe] = 22 μg/mL. The solutions were kept at 45 °C for 10 min, and then the absorbance change was recorded in the plate reader. For fructose, lactose, and maltose, a similar method was used, except glucose was replaced with one of them.

Preparation of Test Strips via Inkjet Printing. A desktop inkjet color printer Epson Workforce 30 was used to print glucose test strips. The standard cyan, magenta, and yellow ink cartridges were replaced with cartridges filled with GOx, chromogenic substrate (ABTS), and Fe_3O_4/MoS_2 solutions. The main reason for choosing this particular printer was its piezoelectric print head, which uses pressure rather than heat because heat can potentially denature GOx. Test strips were developed by printing layers of each solution in the form of a square on the paper and drying at room temperature. Finally, the strips were stored in 4 °C until further use.

Detection of Glucose via Test Strips. Test strips were dipped into a glucose solution of different concentrations for 1 min. After that, it was kept in oven set at 45 °C for 10 min, and the color change was observed with the naked eye.

Calibration of Test Strips. To provide a quantitative assessment, a digital image of the strips was taken using a smartphone (Apple iPhone 6) camera under uniformly distributed lighting conditions that were kept constant throughout all of the experiments. The distance between the camera and strip was also kept constant to maintain consistency. A square block of 1.2 × 1.2 cm^2 was cropped from the digital image of each strip, and the original color pattern was converted into gray scale as well as extracted into red, green, and blue color modes. The absolute intensity values of red, green, blue, and gray were recorded. The change in the intensity (ΔI) pattern was calculated after subtraction of the background (glucose = 0). Calibration plots were made using ΔI of gray scale as well as the mean value red, green, and blue (RGB_{mean}).

RESULTS AND DISCUSSION

The synthesis of monolayer/few layer MoS_2 via liquid exfoliation,[33] chemical vapor deposition (CVD),[53] and physical vapor deposition[54] processes is more suitable for large-scale production compared to mechanical exfoliation.[55] However, chemically exfoliated/grown MoS_2 contains abundant intrinsic and extrinsic structural defects such as sulfur vacancies, point defects, and grain boundaries that have been confirmed via scanning tunneling microscopy, ICP-MS, photoluminescence, and XPS.[30,56−58] Recently, our and several other groups have shown that such surface defects can be passivated by treatment with thiol- or sulfide-containing ligands/compounds.[27−30,59−61] This is due to the reinsertion of missing S atoms at the vacancy sites from a thiol/sulfide group and the formation of disulfide bonds on the MoS_2 surface.[60,62] The ability to passivate sulfur vacancies using a thiol group provides an opportunity to

DOI: 10.1021/acsanm.8b00429
ACS Appl. Nano Mater. XXXX, XXX, XXX−XXX

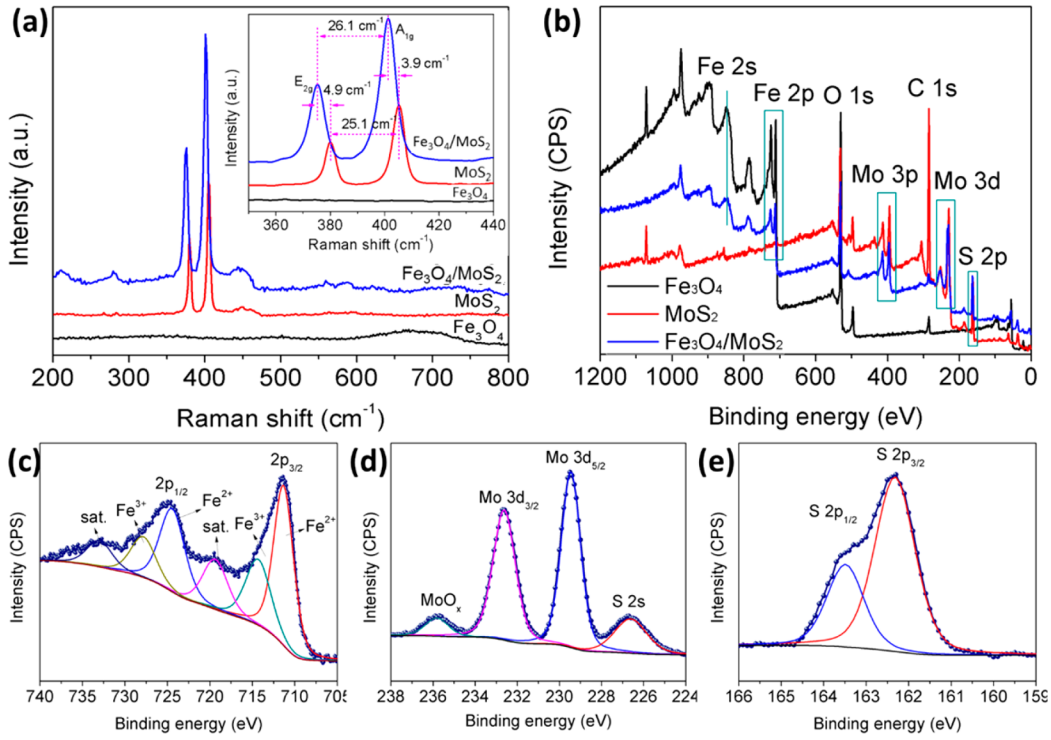

Figure 2. (a) Raman spectroscopy and (b) XPS full-line scan of Fe_3O_4 nanoparticles, MoS_2 nanosheets, and Fe_3O_4/MoS_2 nanocomposites. XPS detailed scans of Fe_3O_4/MoS_2 nanocomposites with characteristic peaks of (c) Fe, (d) Mo, and (e) S.

modulate the surface functionalization of exfoliated MoS_2. In this paper, we have exploited this opportunity to conjugate thiol-functionalized Fe_3O_4 nanoparticles onto MoS_2 nanosheets. Monodisperse thiol-functionalized Fe_3O_4 nanoparticles (size 8 nm) were prepared from oleic acid functionalized Fe_3O_4 nanoparticles via a ligand-exchange process (Figure S1). When bulk MoS_2 was probe-sonicated with the thiol-functionalized Fe_3O_4 nanoparticles, the latter anchored onto exfoliated MoS_2 nanosheets because of thiol affinity toward MoS_2, resulting in Fe_3O_4/MoS_2 nanocomposites (Scheme 1). As a control experiment, when bulk MoS_2 was exfoliated in the presence of citrate-functionalized Fe_3O_4 nanoparticles, there was no integration of Fe_3O_4 nanoparticles on MoS_2 (Figure S2). This confirms that the presence to a thiol group is very critical for the integration of Fe_3O_4 nanoparticles on exfoliated MoS_2 nanosheets during sonication. Also, pristine MoS_2 nanosheets were prepared by sonicating MoS_2 powder with MUA as a stabilizer in water (Figure S3).[51] Figure 1a shows TEM images of Fe_3O_4/MoS_2 nanocomposites, confirming that Fe_3O_4 nanoparticles are decorated on the surface of most of the MoS_2 nanosheets. The apparent aggregation could happen during the TEM sample preparation because slow solvent (water in this case) evaporation induces aggregation during drying. Parts b and c of Figure 1 show the elemental map and EDX pattern of Fe_3O_4/MoS_2. The Fe, Mo, and S signals from the same area confirm the presence of Fe_3O_4 nanoparticles on exfoliated MoS_2 nanosheets. The integration of MoS_2 nanosheets and Fe_3O_4 nanoparticles is also confirmed by Raman spectroscopy and XPS.

Raman spectroscopy can assess the crystallinity and layer thickness of MoS_2 nanosheets in terms of the position and frequency difference of two characteristic vibrational modes, E_{2g} and A_{1g}.[63,64] The E_{2g} mode is attributed to the in-plane vibration of Mo and S atoms, while the A_{1g} mode is related to the out-of-plane vibration of S atoms.[63] Figure 2a shows the Raman spectra of Fe_3O_4/MoS_2 nanocomposites, MoS_2 nanosheets, and Fe_3O_4 nanoparticles dispersed on a Si/SiO_2 substrate. The measurements were conducted using a solid-state laser (532 nm) with a power of 8.8 μW to eliminate the effect of optical heating. The Figure 2a inset shows the two vibrational modes centered at 380.7 and 405.6 cm^{-1}, while the multilayer MoS_2 sheet exhibits modes at 383.8 and 408.6 cm^{-1}. Both spectra give similar E_{2g}-to-A_{1g} frequency differences of ~25 cm^{-1}. This value is smaller than that of bulk MoS_2 but higher than single-layer MoS_2, indicating their exfoliated few-layer structure.[65] Raman spectroscopy has also been utilized to investigate the effect of lattice strain, doping levels, and the van der Waals interaction at the interface of 2D crystals.[63] The in-plane Raman mode, E_{2g}, is sensitive to the built-in strain of 2D MoS_2, while the out-of-plane mode, A_{1g}, is a reflection of interlayer van der Waals interactions. Thus, it is reasonable to predict from the A_{1g} shift of 3.9 cm^{-1} from MoS_2 to Fe_3O_4/MoS_2 that the integration of Fe_3O_4 nanoparticles caused in-plane strain in MoS_2 nanosheets.

XPS was used to determine the chemical composition and chemical states of Fe_3O_4/MoS_2 nanocomposites. As shown in the full-line scans in Figure 2b, the XPS spectra of Fe_3O_4/MoS_2 nanocomposites showed characteristic peaks of both MoS_2 (100−400 eV) and Fe_3O_4 (700−900 eV) nanoparticles, confirming the existence of both MoS_2 and Fe_3O_4 in the nanocomposite. Parts c−e of Figure 2 show detailed scans of Fe_3O_4/MoS_2 nanocomposites with characteristic peaks of Fe, Mo, and S. The spectrum in the Fe $2p_{3/2}$ region can be deconvoluted into two main peaks and a satellite peak (Figure 2c). The same pattern is repeated, with almost half-intensity for the $2p_{1/2}$ component. Fe_3O_4 comprises two oxidation states, Fe^{2+} and Fe^{3+}. The lowest binding energy peak at 710.2 eV is attributed to Fe^{2+}, with a corresponding satellite at 718.0 eV.

DOI: 10.1021/acsanm.8b00429
ACS Appl. Nano Mater. XXXX, XXX, XXX−XXX

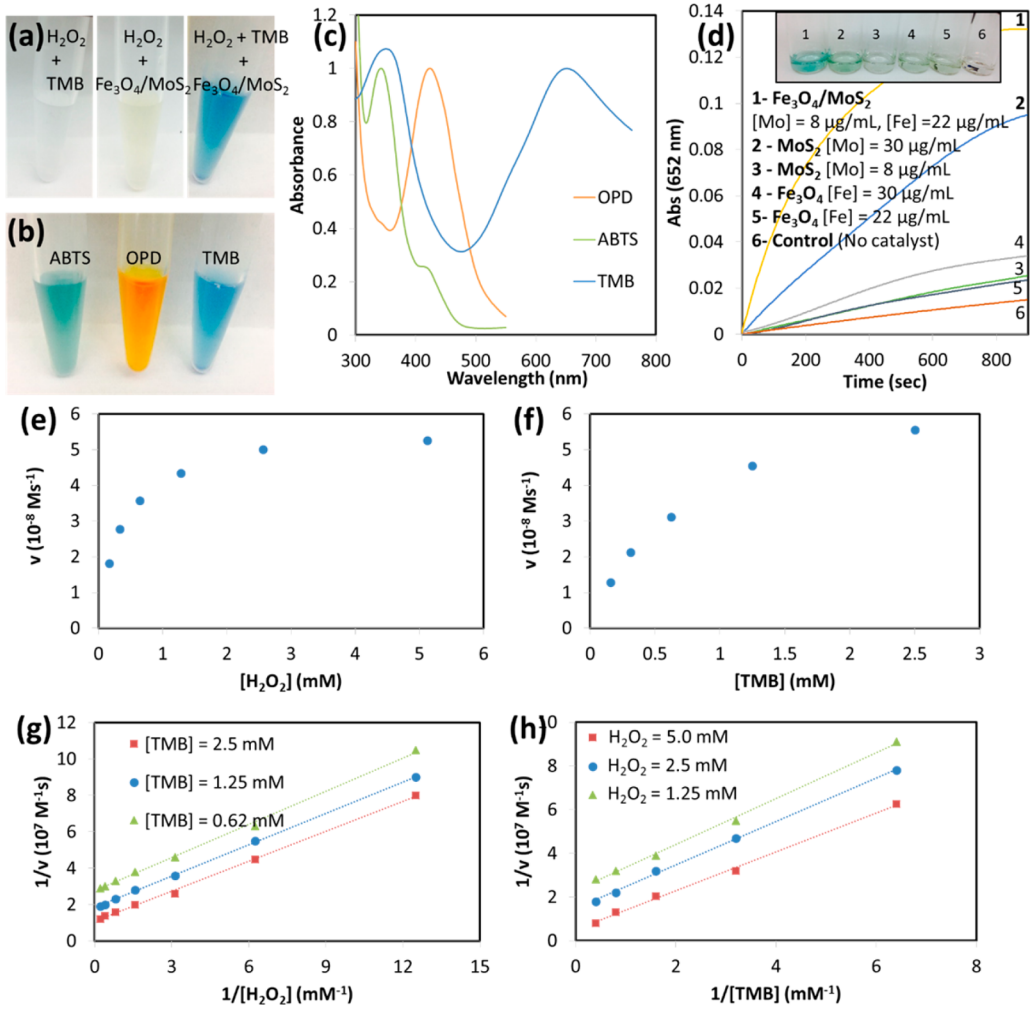

Figure 3. (a) Demonstration of the peroxidase-like activity of Fe_3O_4/MoS_2 ([Mo] = 8 μg/mL; [Fe] = 22 μg/mL) nanocomposites in the presence of 100 mM H_2O_2 and 1.25 mM TMB. Color change was only observed in a solution of H_2O_2 + TMB + Fe_3O_4/MoS_2, while solutions of H_2O_2 + TMB and H_2O_2 + Fe_3O_4/MoS_2 remained colorless. Similar to TMB, the other chromogenic substrates such as 1 mM ABTS and 1 mM OPD were also oxidized and resulted in green and orange color, respectively. (b) Picture and (c) absorbance plots of oxidized substrates (ABTS, OPD, and TMB) in the presence of H_2O_2. (d) Reaction kinetics of Fe_3O_4/MoS_2 in comparison to MoS_2 and Fe_3O_4 in the presence of 2.5 mM H_2O_2 and 1.25 mM TMB. (e and f) Initial velocity (v) plots via a steady-state kinetic assay of Fe_3O_4/MoS_2. The velocity of the reaction was measured in a 0.1 M citrate phosphate buffer (pH 5.0) at room temperature. The concentrations of Fe_3O_4/MoS_2 were chosen as [Mo] = 8 μg/mL and [Fe] = 22 μg/mL. The concentration of TMB in part e was kept at 1.25 mM, and the H_2O_2 concentration was varied. (f) The concentration of TMB in part f was kept at 2.5 mM, and the TMB concentration was varied. (g and h) Double-reciprocal plots of the catalytic activity of Fe_3O_4/MoS_2 at three sets of fixed concentration of one substrate (H_2O_2 or TMB) while the other was varied.

The Fe^{3+} peak is found with a binding energy of 713.3 eV. The peak positions of Fe $2p_{3/2}$ and Fe $2p_{1/2}$ are comparable to the reported values in the literature.[66−68] Figure 2d displays Mo 3d peaks at 233.04 and 229.87 eV, corresponding to the $3d_{5/2}$ and $3d_{3/2}$ doublets. The S 2p peak can be deconvoluted into two peaks at 163.88 and 162.70 eV (Figure 2e), attributed to the $2p_{1/2}$ and $2p_{3/2}$ orbitals. These binding energy values confirm the charge states of Mo and S in the MoS_2 nanosheets to be Mo^{4+} and S^{2-}, which is consistent with previous reports.[64,69] No additional peaks of metallic Mo or MoO_x in the higher- and lower-binding-energy regions confirm that the exfoliated MoS_2 nanosheets are quality similar to CVD-grown MoS_2.[70]

Fe_3O_4 nanoparticles have been shown as a robust alternative of horseradish peroxidase (HRP) because of their intrinsic peroxidase-like properties, lower cost, and higher chemical stability.[41,71,72] We have explored the peroxidase-like catalytic activity of Fe_3O_4/MoS_2 nanocomposites based on the reports that 0D/2D nanocomposites show better catalytic ability compared to 0D nanoparticles alone.[34,35] Fe_3O_4/MoS_2 nanocomposites mixed with a solution of chromogenic substrate TMB and H_2O_2 turn blue within seconds, while control solutions (H_2O_2 + TMB or H_2O_2 + Fe_3O_4/MoS_2) show a negligible color change, confirming the peroxidase-like catalytic activity of Fe_3O_4/MoS_2 nanocomposites (Figure 3a). Similar behavior was observed for other chromogenic substrates such as ABTS and OPD, resulting in green and orange color, respectively (Figure 3b). The absorbance plots confirm that characteristic peaks of oxidized TMB, ABTS, and OPD are observed (Figure 3c).[73] On the basis of kinetic studies of Fe_3O_4/MoS_2 nanocomposites (Figure S4), the peroxidase-like activity was further investigated. The initial velocities from the steady-state kinetic plots were obtained at different concentrations of H_2O_2 while keeping TMB constant or vice versa (Figure 3e,f). The oxidation reaction catalyzed by Fe_3O_4/MoS_2 nanocomposites follows the typical Michaelis−Menten pattern for both substrates, H_2O_2 and TMB.[34,36,37,41,48] The double-

DOI: 10.1021/acsanm.8b00429
ACS Appl. Nano Mater. XXXX, XXX, XXX−XXX

reciprocal plots of the initial velocity against one of the substrate concentrations were also acquired when the other substrate was fixed at three concentrations (Figure 3g,h). The calculated velocity was applied to the Lineweaver–Burk plot, which is

$$\frac{1}{v} = \left(\frac{K_m}{V_{max}}\right)\frac{1}{[S]} + \frac{1}{V_{max}} \quad (1)$$

where v is the initial velocity, K_m is the Michaelis–Menten constant, V_{max} is the maximal reaction velocity, and [S] is the concentration of the substrate.[34,36,37,41,48] The calculated K_m and V_{max} values from eq 1 are shown in Table 1. The slopes of the lines in the reciprocal plots are parallel at all three concentrations, indicating a ping-pong mechanism, characteristic of HRP, and this indicates that Fe_3O_4/MoS_2 nanocomposites bind and react with the first substrate, release the first product, and then react with the second substrate.[34,36,37,41,48]

Table 1. Comparison of the K_m and V_{max} Values of Fe_3O_4/MoS_2 with HRP and Other Peroxidase-Like Catalysts

catalyst	substrate	K_m ($\times 10^{-3}$ M)	V_{max} ($\times 10^{-8}$ M/s)	ref
Fe_3O_4/MoS_2 nanocomposite	H_2O_2	0.32	5.56	this work
	TMB	0.62	6.25	this work
HRP	H_2O_2	3.7	8.71	41
	TMB	0.434	10.0	41
MoS_2 nanosheets	H_2O_2	0.0116	4.29	37
	TMB	0.52	5.16	37
Fe_3O_4 nanoparticles	H_2O_2	154	9.78	41
	TMB	0.098	3.44	41

To compare the catalytic activity of Fe_3O_4/MoS_2, the apparent K_m and V_{max} values are listed with HRP and other previously reported MoS_2 or Fe_3O_4-based peroxidase-like catalysts in Table 1. The lower K_m value shows the higher affinity of the peroxidase catalyst toward the substrate, while the higher V_{max} values show the higher catalytic ability of the catalyst. The apparent K_m value of Fe_3O_4/MoS_2 nanocomposites with H_2O_2 as the substrate is significantly lower than that of HRP and Fe_3O_4, indicating that Fe_3O_4/MoS_2 has a higher affinity than HRP and Fe_3O_4 nanoparticles toward H_2O_2. In other words, a lower H_2O_2 concentration is required for the Fe_3O_4/MoS_2 nanocomposites than for HRP or Fe_3O_4 nanoparticles for maximum catalytic activity. The lower affinity (high K_m) of Fe_3O_4/MoS_2 for TMB can also guarantee that more active sites would be available for H_2O_2. In comparison to MoS_2 nanosheets though, Fe_3O_4/MoS_2 nanocomposites show higher K_m (low affinity), but a higher V_{max} value is observed for both TMB and H_2O_2. The higher V_{max} value can be associated with increased catalytic sites provided by the integration of Fe_3O_4 nanoparticles on large-area MoS_2 nanosheets.[34] The enhanced peroxidase-like catalytic activity is further confirmed by the faster steady-state reaction kinetics of the Fe_3O_4/MoS_2 nanocomposites in comparison to the similar concentrations of Fe_3O_4 nanoparticles and MoS_2 nanosheets (Figure 3d).[41] The increased catalytic activity confirms that integration of Fe_3O_4 nanoparticles on MoS_2 nanosheets results in synergistic effects, which result in a higher catalytic ability of Fe_3O_4/MoS_2 nanocomposites compared to their single-phase counterparts. This is similar to previous reports in which 0D/2D nanocomposites have demonstrated enhanced thermal, electronic, and catalytic properties because of the synergistic effects generated from the outstanding physical properties of the nanoparticles on the unique 2D morphology.[7−18] Using the intrinsic peroxidase-like activity, H_2O_2 was detected in a linear range from 1.25 to 40 μM and LOD was found to be 0.8 μM (Figure S5).[24]

On the basis of the intrinsic peroxidase-like activity, a colorimetric method of glucose detection was developed. The reaction is based on a color change of a substrate (such as TMB) when it is mixed with glucose and GOx and catalyzed by a peroxidase-active catalyst (Figure 4a).[72,74] Here we have used Fe_3O_4/MoS_2 as the peroxidase-active catalyst. When GOx, TMB, and Fe_3O_4/MoS_2 are mixed with glucose solutions, they turn blue in a dose-dependent manner, validating the glucose detection ability of Fe_3O_4/MoS_2. The change in color is quantified by measuring the absorbance at 652 nm. Figure 4b shows the absorbance recorded at glucose concentrations of 5–150 μM, which shows a linear response. The LOD was calculated from the standard deviation of the blank and glucose linear response curve and was found to be 2.4 μM. The glucose detection ability of Fe_3O_4/MoS_2 nanocomposites was found to be significantly higher compared to Fe_3O_4 nanoparticles and MoS_2 nanosheets with similar Mo and Fe concentrations, respectively (Figure S6). Table 2 shows a comparison of the

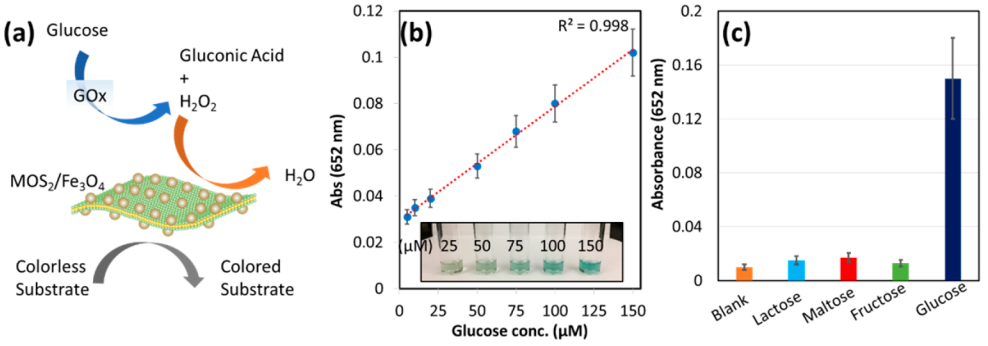

Figure 4. (a) Schematic of glucose detection via Fe_3O_4/MoS_2. (b) Dose-dependent behavior for glucose detection in the presence of GOx, TMB, and Fe_3O_4/MoS_2. The absorbance values recorded from 5 to 150 μM glucose in the presence of GOx (3.33 mg/mL), TMB (1.25 mM), and Fe_3O_4/MoS_2 ([Mo] = 8 μg/mL; [Fe] = 22 μg/mL) show a linear response. (c) Selectivity analysis of our detection method by monitoring the absorbance of glucose and its analogues—fructose, lactose, and maltose—in the presence of GOx (3.33 mg/mL), TMB (1.25 mM), and Fe_3O_4/MoS_2 ([Mo] = 8 μg/mL; [Fe] = 22 μg/mL). The change in the absorbance in only a glucose solution demonstrates the highly selective nature of our method.

DOI: 10.1021/acsanm.8b00429
ACS Appl. Nano Mater. XXXX, XXX, XXX−XXX

Table 2. Comparison of the Glucose Detection Linear Range and LOD Values of Fe_3O_4/MoS_2 with Other Peroxidase-Like Catalysts

catalyst	range (μM)	LOD (μM)	ref
Fe_3O_4/MoS_2	5−150	2.4	this work
Fe_3O_4	50−1000	30	24
MoS_2	5−150	1.2	37
GO	1−20	1.0	36
GO/Fe_3O_4	2−200	0.74	34
WS_2	5−300	2.9	48
CeO_2	4−40	2.0	40
PVP/MoS_2	10^3−10^4	320	46
Au^+	18−1100	4	45
Au@*p*-SiO_2	20−500	20	75
Hemin@MOF	10−300	N/A	76

glucose detection linear range and LOD value of Fe_3O_4/MoS_2 with those of previously reported peroxidase-like catalysts, which confirms that Fe_3O_4/MoS_2 nanocomposites show a similar or better response than previous glucose-sensing platforms.[24,34,36,37,40,45,46,48,75,76] After glucose was replaced with fructose, lactose, and maltose, the negligible change in the absorbance at 652 nm demonstrates the highly selective nature of our glucose detection method (Figure 4c).

For the diagnosis of diseases like diabetes, monitoring of glucose is the standard method. Most glucose sensing is done by a conventional glucometer, where a drop of blood is deposited onto an enzymatic test strip and the glucose concentration is electrochemically detected.[72] For monitoring of glucose levels throughout a day, users have to prick their fingers multiple times, which results in discomfort, pain, possible fainting, and risk of infection. Also, in developing countries with low-resource settings, it is even more challenging to have access to conventional glucose diagnoses. Hence, a simple, noninvasive, and accessible tool/technique for monitoring of glucose levels is necessary. Utilizing the high chemical stability and superior colorimetric detection ability of Fe_3O_4/MoS_2 nanocomposites, we have developed a noninvasive point-of-care diagnostic platform for quick, convenient, and pain-free glucose detection. Paper-based "dip and use" test strips have been developed that show a colorimetric response when dipped into aqueous glucose solutions. To prepare test strips, square block layers of GOx, chromogenic substrate, and Fe_3O_4/MoS_2 are printed on a desktop inkjet printer.[77] ABTS was chosen as the chromogenic substrate because of its better color contrast with paper strips compared to OPD and TMB at similar concentrations. After dipping into a glucose solution for 1 min and heating of the strip at 45 °C for 10 min, the block's color changes from colorless to green (Figure 5a). The intensity of the color is dependent on the concentration of the glucose solution (Figure 5b). The test strips enable visual detection of glucose as low as 12.5 mM or 225 mg/dL. The dose-dependent color change provides a qualitative assessment that is sufficient to distinguish the glucose concentration in healthy (3−8 mM) and diabetic (9−40 mM) persons.[78] The noticeable color change with the naked eye establishes the effectiveness of the colorimetric test-strip platform. Further, by providing a

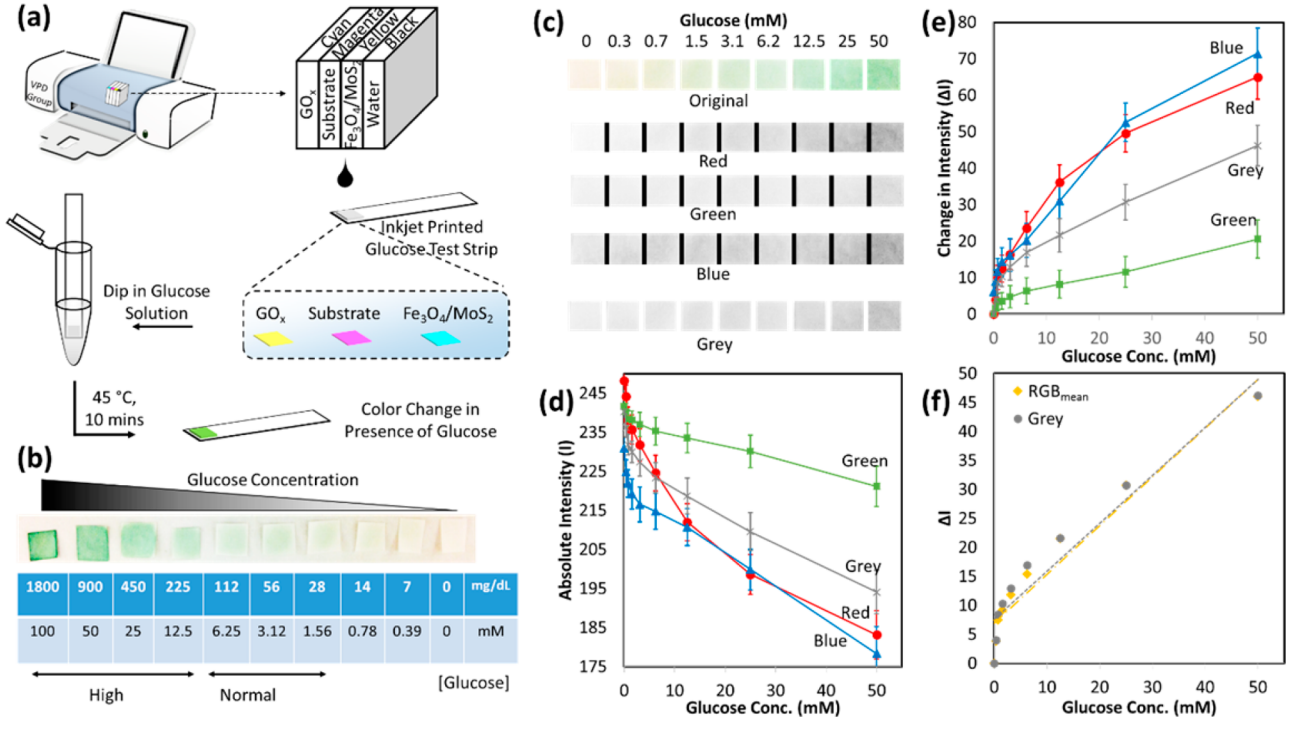

Figure 5. (a) Development of glucose test strips (for transparent analytes such as sweat, saliva, tear, or urine) by inkjet printing solutions of GOx (3.33 mg/mL), ABTS (1.25 mM), and Fe_3O_4/MoS_2 ([Mo] = 8 μg/mL; [Fe] = 22 μg/mL). The strip turns colorless to green in the presence of different concentrations of glucose solutions. (b) Strips showing an increase in the green color intensity with increasing glucose concentration. An image of the strips after a color change is taken using a digital camera under uniformly distributed lighting conditions. (c) Square block of 1.2 × 1.2 cm^2 cropped from the digital image of each strip for quantitative assessment. The original color pattern was extracted into red, green, and blue color modes as well as gray-scale mode. (d) Absolute intensity values of red, green, blue, and gray color modes recorded using Photoshop. (e) ΔI pattern calculated after subtraction of the background (glucose = 0). (f) Calibration plots made using ΔI values of gray scale as well as RGB_{mean}. Both calibration plots match very well.

DOI: 10.1021/acsanm.8b00429
ACS Appl. Nano Mater. XXXX, XXX, XXX−XXX

reference strip as part of the test kit, subjectivity of the color change can be further reduced by comparing the test strip with the reference one.

To provide quantitative assessment, a digital image of the strips after color change is taken using a smartphone (Apple iPhone 6) camera under uniformly distributed lighting conditions that were kept constant for all of the experiments. A square block of 1.2 × 1.2 cm^2 is cropped from the digital image of each strip, and the original color pattern is converted into gray scale as well as extracted into red, green, and blue color modes (Figure 5c). The absolute intensity values of red, green, blue, and gray color modes are recorded (Figure 5d). The ΔI pattern is plotted after subtraction of the background (glucose = 0) and is found to be proportional to the glucose concentration (Figure 5e). To calculate unknown concentrations of glucose, calibration plots are made using ΔI values of gray scale as well as RGB_{mean} (Figure 5f). Both calibration plots match very well and can be used to quantify the glucose concentration based on the color of the strip. We believe the colorimetric detection of glucose from the test strips made of Fe_3O_4/MoS_2 composites can be used for quick determination of the glucose concentration in body fluids such as saliva, tear, sweat, and urine. Because the direct correlation between saliva and blood glucose has been reported, the strips can be a powerful tool for the noninvasive detection of blood glucose levels.[79−81] The same is possible using tear, sweat, and urine once the correlation of tear (or sweat or urine) and blood glucose is established. The strips can be extremely useful in developing world areas with low or no diagnostic resources. In an advanced version, we are working on a process that can digitize the results in order to read them on a portable device. Efforts to improve the sensitivity of the test strips and to adapt the methodology for detection of other biomolecules in body fluids as well as toxic elements in the environment are ongoing.

SUMMARY AND CONCLUSIONS

We have demonstrated a one-pot ecofriendly approach to synthesize 0D/2D nanocomposites and their applications toward noninvasive point-of-care diagnostics. Fe_3O_4/MoS_2 nanocomposites have been prepared by exfoliating MoS_2 in an aqueous dispersion of thiol-functionalized Fe_3O_4 nanoparticles. The method is versatile and has the potential to generate a library of 0D/2D nanocomposites by choosing different 2D materials and nanoparticles with the appropriate functionality. Because of the unique 0D/2D morphology, Fe_3O_4/MoS_2 nanocomposites show excellent peroxidase-like catalytic activity that is superior to either MoS_2 nanosheets or Fe_3O_4 nanoparticles alone. The enhanced catalytic activity is utilized to colorimetrically detect glucose via absorbance measurements, with the LOD equal to 2.4 μM. A noninvasive point-of-care diagnostic platform is established for quick, convenient, and pain-free glucose detection. By inkjet printing Fe_3O_4/MoS_2 nanocomposites, paper-based test strips are developed that change their color in the presence of glucose solutions and allow the visual detection of glucose concentrations that is sufficient enough to distinguish between normal (healthy) and high (diabetic) glucose levels. Because of their easy preparation, chemical stability, and excellent catalytic ability, Fe_3O_4/MoS_2 nanocomposites show great potential toward the development of medical and environmental diagnostic tools.

ASSOCIATED CONTENT

Supporting Information

The Supporting Information is available free of charge on the ACS Publications website at DOI: 10.1021/acsanm.8b00429.

TEM images of Fe_3O_4 nanoparticles and SDS-stabilized MoS_2 nanosheets, citrate-functionalized Fe_3O_4 nanoparticles and MoS_2 nanosheets, reaction kinetics of different concentrations of Fe_3O_4/MoS_2, and absorbance plots (PDF)

AUTHOR INFORMATION

Corresponding Author

*E-mail: v-dravid@northwestern.edu.

ORCID

Vikas Nandwana: 0000-0002-7088-8813

Yuan Li: 0000-0001-7452-1149

Vinayak P. Dravid: 0000-0002-6007-3063

Notes

The authors declare no competing financial interest.

ACKNOWLEDGMENTS

V.N. and V.P.D. gratefully acknowledge support from the NTU-NU Institute for NanoMedicine located at the International Institute for Nanotechnology, Northwestern University, and the Nanyang Technological University, Singapore. Research related to oxide nanostructures was also supported by the National Science Foundation (NSF) under Grant DMR-1507810. This work made use of the EPIC and Keck-II facilities of the NUANCE Center at Northwestern University, which received support from the Soft and Hybrid Nanotechnology Experimental Resource (NSF Grant NNCI-1542205), the MRSEC program (NSF Grant DMR-1720139) at the Materials Research Center, the IIN, the Keck Foundation, and the State of Illinois, through the IIN.

REFERENCES

(1) Li, X.; Shan, J. Y.; Zhang, W. Z.; Su, S.; Yuwen, L. H.; Wang, L. H. Recent Advances in Synthesis and Biomedical Applications of Two-Dimensional Transition Metal Dichalcogenide Nanosheets. *Small* **2017**, *13*, 1602660.

(2) Deng, D. H.; Novoselov, K. S.; Fu, Q.; Zheng, N. F.; Tian, Z. Q.; Bao, X. H. Catalysis with Two-dimensional Materials and Their Heterostructures. *Nat. Nanotechnol.* **2016**, *11*, 218−230.

(3) Lv, R.; Robinson, J. A.; Schaak, R. E.; Sun, D.; Sun, Y. F.; Mallouk, T. E.; Terrones, M. Transition Metal Dichalcogenides and Beyond: Synthesis, Properties, and Applications of Single- and Few-Layer Nanosheets. *Acc. Chem. Res.* **2015**, *48*, 56−64.

(4) Xu, M. S.; Liang, T.; Shi, M. M.; Chen, H. Z. Graphene-Like Two-Dimensional Materials. *Chem. Rev.* **2013**, *113*, 3766−3798.

(5) Tan, C. L.; Cao, X. H.; Wu, X. J.; He, Q. Y.; Yang, J.; Zhang, X.; Chen, J. Z.; Zhao, W.; Han, S. K.; Nam, G. H.; Sindoro, M.; Zhang, H. Recent Advances in Ultrathin Two-Dimensional Nanomaterials. *Chem. Rev.* **2017**, *117*, 6225−6331.

(6) Zhang, X.; Lai, Z. C.; Tan, C. L.; Zhang, H. Solution-Processed Two-Dimensional MoS2 Nanosheets: Preparation, Hybridization, and Applications. *Angew. Chem., Int. Ed.* **2016**, *55*, 8816−8838.

(7) Xiang, Q. J.; Yu, J. G.; Jaroniec, M. Synergetic Effect of MoS2 and Graphene as Cocatalysts for Enhanced Photocatalytic H-2 Production Activity of TiO2 Nanoparticles. *J. Am. Chem. Soc.* **2012**, *134*, 6575−6578.

(8) Kufer, D.; Nikitskiy, I.; Lasanta, T.; Navickaite, G.; Koppens, F. H. L.; Konstantatos, G. Hybrid 2D-0D MoS2-PbS Quantum Dot Photodetectors. *Adv. Mater.* **2015**, *27*, 176−180.

DOI: 10.1021/acsanm.8b00429
ACS Appl. Nano Mater. XXXX, XXX, XXX−XXX

(9) Ahmad, R.; Srivastava, R.; Yadav, S.; Singh, D.; Gupta, G.; Chand, S.; Sapra, S. Functionalized Molybdenum Disulfide Nanosheets for 0D-2D Hybrid Nanostructures: Photoinduced Charge Transfer and Enhanced Photoresponse. *J. Phys. Chem. Lett.* **2017**, *8*, 1729−1738.
(10) Li, Y. G.; Wang, H. L.; Xie, L. M.; Liang, Y. Y.; Hong, G. S.; Dai, H. J. MoS2 Nanoparticles Grown on Graphene: An Advanced Catalyst for the Hydrogen Evolution Reaction. *J. Am. Chem. Soc.* **2011**, *133*, 7296−7299.
(11) Xu, S. J.; Li, D.; Wu, P. Y. One-Pot, Facile, and Versatile Synthesis of Monolayer MoS2/WS2 Quantum Dots as Bioimaging Probes and Efficient Electrocatalysts for Hydrogen Evolution Reaction. *Adv. Funct. Mater.* **2015**, *25*, 1127−1136.
(12) Song, H. J.; You, S. S.; Jia, X. H.; Yang, J. MoS2 Nanosheets Decorated with Magnetic Fe3O4 Nanoparticles and Their Ultrafast Adsorption for Wastewater Treatment. *Ceram. Int.* **2015**, *41*, 13896−13902.
(13) Kabachii, Y. A.; Golub, A. S.; Kochev, S. Y.; Lenenko, N. D.; Abramchuk, S. S.; Antipin, M. Y.; Valetsky, P. M.; Stein, B. D.; Mahmoud, W. E.; Al-Ghamdi, A. A.; Bronstein, L. M. Multifunctional Nanohybrids by Self-Assembly of Monodisperse Iron Oxide Nanoparticles and Nanolamellar MoS2 Plates. *Chem. Mater.* **2013**, *25*, 2434−2440.
(14) Liu, T.; Shi, S. X.; Liang, C.; Shen, S. D.; Cheng, L.; Wang, C.; Song, X. J.; Goel, S.; Barnhart, T. E.; Cai, W. B.; Liu, Z. Iron Oxide Decorated MoS2 Nanosheets with Double PEGylation for Chelator-Free Radio Labeling and Multimodal Imaging Guided Photothermal Therapy. *ACS Nano* **2015**, *9*, 950−960.
(15) Yu, J.; Yin, W. Y.; Zheng, X. P.; Tian, G.; Zhang, X.; Bao, T.; Dong, X. H.; Wang, Z. L.; Gu, Z. J.; Ma, X. Y.; Zhao, Y. L. Smart MoS2/Fe3O4 Nanotheranostic for Magnetically Targeted Photothermal Therapy Guided by Magnetic Resonance/Photoacoustic Imaging. *Theranostics* **2015**, *5*, 931−945.
(16) Chen, Y.; Song, B. H.; Tang, X. S.; Lu, L.; Xue, J. M. Ultrasmall Fe3O4 Nanoparticle/MoS2 Nanosheet Composites with Superior Performances for Lithium Ion Batteries. *Small* **2014**, *10*, 1536−1543.
(17) Lin, T. R.; Wang, J.; Guo, L. Q.; Fu, F. F. Fe3O4@MoS2 Core-Shell Composites: Preparation, Characterization, and Catalytic Application. *J. Phys. Chem. C* **2015**, *119*, 13658−13664.
(18) Wu, H. C.; Coileain, C. O.; Abid, M.; Mauit, O.; Syrlybekov, A.; Khalid, A.; Xu, H. J.; Gatensby, R.; Wang, J. J.; Liu, H. J.; Yang, L.; Duesberg, G. S.; Zhang, H. Z.; Abid, M.; Shvets, I. V. Spin-Dependent Transport Properties of Fe3O4/MoS2/Fe3O4 Junctions. *Sci. Rep.* **2015**, *5*, 15984.
(19) Nandwana, V.; De, M.; Chu, S.; Jaiswal, M.; Rotz, M.; Meade, T. J.; Dravid, V. P. Nanotechnology-based Precision Tools for the Detection and Treatment of Cancer. In. *Cancer Treat. Res.* **2015**, *166*, 51−83.
(20) Nandwana, V.; Ryoo, S. R.; Kanthala, S.; De, M.; Chou, S. S.; Prasad, P. V.; Dravid, V. P. Engineered Theranostic Magnetic Nanostructures: Role of Composition and Surface Coating on Magnetic Resonance Imaging Contrast and Thermal Activation. *ACS Appl. Mater. Interfaces* **2016**, *8*, 6953−6961.
(21) Lee, N.; Yoo, D.; Ling, D.; Cho, M. H.; Hyeon, T.; Cheon, J. Iron Oxide Based Nanoparticles for Multimodal Imaging and Magnetoresponsive Therapy. *Chem. Rev.* **2015**, *115*, 10637−10689.
(22) Laurent, S.; Forge, D.; Port, M.; Roch, A.; Robic, C.; Vander Elst, L.; Muller, R. N. Magnetic Iron Oxide Nanoparticles: Synthesis, Stabilization, Vectorization, Physicochemical Characterizations, and Biological Applications. *Chem. Rev.* **2008**, *108*, 2064−2110.
(23) Xu, P. A.; Zeng, G. M.; Huang, D. L.; Feng, C. L.; Hu, S.; Zhao, M. H.; Lai, C.; Wei, Z.; Huang, C.; Xie, G. X.; Liu, Z. F. Use of Iron Oxide Nanomaterials in Wastewater Treatment: A review. *Sci. Total Environ.* **2012**, *424*, 1−10.
(24) Wei, H.; Wang, E. Fe3O4Magnetic Nanoparticles as Peroxidase Mimetics and their Applications in H2O2 and Glucose Detection. *Anal. Chem.* **2008**, *80*, 2250−2254.
(25) Zeng, H.; Li, J.; Liu, J. P.; Wang, Z. L.; Sun, S. H. Exchange-coupled Nanocomposite Magnets by Nanoparticle Self-assembly. *Nature* **2002**, *420*, 395−398.
(26) Zhang, H.; Nikolov, A.; Wasan, D. Enhanced Oil Recovery (EOR) Using Nanoparticle Dispersions: Underlying Mechanism and Imbibition Experiments. *Energy Fuels* **2014**, *28*, 3002−3009.
(27) Chou, S. S.; De, M.; Kim, J.; Byun, S.; Dykstra, C.; Yu, J.; Huang, J. X.; Dravid, V. P. Ligand Conjugation of Chemically Exfoliated MoS2. *J. Am. Chem. Soc.* **2013**, *135*, 4584−4587.
(28) Wang, Y.; Qi, L.; Shen, L.; Wu, Y. H. Surface Defect Passivation of MoS2 by Sulfur, Selenium, and Tellurium. *J. Appl. Phys.* **2016**, *119*, 154301.
(29) Tuxen, A.; Kibsgaard, J.; Gobel, H.; Laegsgaard, E.; Topsøe, H.; Lauritsen, J. V.; Besenbacher, F. Size Threshold in the Dibenzothiophene Adsorption on MoS2 Nanoclusters. *ACS Nano* **2010**, *4*, 4677−4682.
(30) Sim, D. M.; Kim, M.; Yim, S.; Choi, M. J.; Choi, J.; Yoo, S.; Jung, Y. S. Controlled Doping of Vacancy-Containing Few-Layer MoS2 via Highly Stable Thiol-Based Molecular Chemisorption. *ACS Nano* **2015**, *9*, 12115−12123.
(31) Nicolosi, V.; Chhowalla, M.; Kanatzidis, M. G.; Strano, M. S.; Coleman, J. N. Liquid Exfoliation of Layered Materials. *Science* **2013**, *340*, 1226419.
(32) Coleman, J. N. Liquid Exfoliation of Defect-Free Graphene. *Acc. Chem. Res.* **2013**, *46*, 14−22.
(33) Coleman, J. N.; Lotya, M.; O'Neill, A.; Bergin, S. D.; King, P. J.; Khan, U.; Young, K.; Gaucher, A.; De, S.; Smith, R. J.; Shvets, I. V.; Arora, S. K.; Stanton, G.; Kim, H. Y.; Lee, K.; Kim, G. T.; Duesberg, G. S.; Hallam, T.; Boland, J. J.; Wang, J. J.; Donegan, J. F.; Grunlan, J. C.; Moriarty, G.; Shmeliov, A.; Nicholls, R. J.; Perkins, J. M.; Grieveson, E. M.; Theuwissen, K.; McComb, D. W.; Nellist, P. D.; Nicolosi, V. Two-Dimensional Nanosheets Produced by Liquid Exfoliation of Layered Materials. *Science* **2011**, *331*, 568−571.
(34) Dong, Y. L.; Zhang, H. G.; Rahman, Z. U.; Su, L.; Chen, X. J.; Hu, J.; Chen, X. G. Graphene Oxide-Fe3O4Magnetic Nanocomposites with Peroxidase-like Activity for Colorimetric Detection of Glucose. *Nanoscale* **2012**, *4*, 3969−3976.
(35) Vashist, S. K.; Luong, J. H. T. Recent Advances in Electrochemical Biosensing Schemes using Graphene and Graphene-based Nanocomposites. *Carbon* **2015**, *84*, 519−550.
(36) Song, Y. J.; Qu, K. G.; Zhao, C.; Ren, J. S.; Qu, X. G. Graphene Oxide: Intrinsic Peroxidase Catalytic Activity and Its Application to Glucose Detection. *Adv. Mater.* **2010**, *22*, 2206−2210.
(37) Lin, T. R.; Zhong, L. S.; Guo, L. Q.; Fu, F. F.; Chen, G. N. Seeing Diabetes: Visual Detection of Glucose based on the Intrinsic Peroxidase-like Activity of MoS2 Nanosheets. *Nanoscale* **2014**, *6*, 11856−11862.
(38) Sun, Z.; Zhao, Q. S.; Zhang, G. H.; Li, Y.; Zhang, G. L.; Zhang, F. B.; Fan, X. B. Exfoliated MoS2 Supported Au-Pd Bimetallic Nanoparticles with Core-shell Structures and Superior Peroxidase-like Activities. *RSC Adv.* **2015**, *5*, 10352−10357.
(39) Cai, S. F.; Han, Q. S.; Qi, C.; Lian, Z.; Jia, X. H.; Yang, R.; Wang, C. Pt74Ag26 nanoparticle-decorated ultrathin MoS2 nanosheets as novel peroxidase mimics for highly selective colorimetric detection of H2O2 and glucose. *Nanoscale* **2016**, *8*, 3685−3693.
(40) Guo, R. C.; Wang, Y. R.; Yu, S. X.; Zhu, W. X.; Zheng, F. Q.; Liu, W.; Zhang, D. H.; Wang, J. L. Dual Role of Hydrogen Peroxide on the Oxidase-like Activity of Nanoceria and its Application for Colorimetric Hydrogen Peroxide and Glucose Sensing. *RSC Adv.* **2016**, *6*, 59939−59945.
(41) Gao, L. Z.; Zhuang, J.; Nie, L.; Zhang, J. B.; Zhang, Y.; Gu, N.; Wang, T. H.; Feng, J.; Yang, D. L.; Perrett, S.; Yan, X. Intrinsic Peroxidase-like Activity of Ferromagnetic Nanoparticles. *Nat. Nanotechnol.* **2007**, *2*, 577−583.
(42) Wang, T. Y.; Zhu, H. C.; Zhuo, J. Q.; Zhu, Z. W.; Papakonstantinou, P.; Lubarsky, G.; Lin, J.; Li, M. X. Biosensor Based on Ultrasmall MoS2 Nanoparticles for Electrochemical Detection of H2O2 Released by Cells at the Nanomolar Level. *Anal. Chem.* **2013**, *85*, 10289−10295.
(43) Tao, Y.; Lin, Y. H.; Huang, Z. Z.; Ren, J. S.; Qu, X. G. Incorporating Graphene Oxide and Gold Nanoclusters: A Synergistic Catalyst with Surprisingly High Peroxidase-Like Activity Over a Broad

DOI: 10.1021/acsanm.8b00429
ACS Appl. Nano Mater. XXXX, XXX, XXX−XXX

pH Range and its Application for Cancer Cell Detection. *Adv. Mater.* **2013**, *25*, 2594−2599.
(44) Li, B. L.; Luo, H. Q.; Lei, J. L.; Li, N. B. Hemin-functionalized MoS2 Nanosheets: Enhanced Peroxidase-like Catalytic Activity with a Steady State in Aqueous Solution. *RSC Adv.* **2014**, *4*, 24256−24262.
(45) Jv, Y.; Li, B. X.; Cao, R. Positively-charged Gold Nanoparticles as Peroxidiase Mimic and Their Application in Hydrogen Peroxide and Glucose Detection. *Chem. Commun.* **2010**, *46*, 8017−8019.
(46) Yu, J.; Ma, X. Y.; Yin, W. Y.; Gu, Z. J. Synthesis of PVP-functionalized Ultra-small MoS2 Nanoparticles with Intrinsic Peroxidase-Like Activity for H2O2 and Glucose Detection. *RSC Adv.* **2016**, *6*, 81174−81183.
(47) Lin, T. R.; Zhong, L. S.; Wang, J.; Guo, L. Q.; Wu, H. Y.; Guo, Q. Q.; Fu, F. F.; Chen, G. N. Graphite-like Carbon Nitrides as Peroxidase Mimetics and Their Applications to Glucose Detection. *Biosens. Bioelectron.* **2014**, *59*, 89−93.
(48) Lin, T. R.; Zhong, L. S.; Song, Z. P.; Guo, L. Q.; Wu, H. Y.; Guo, Q. Q.; Chen, Y.; Fu, F. F.; Chen, G. N. Visual Detection of Blood Glucose Based on Peroxidase-like Activity of WS2 Nanosheets. *Biosens. Bioelectron.* **2014**, *62*, 302−307.
(49) Zhao, K.; Gu, W.; Zheng, S. S.; Zhang, C. L.; Xian, Y. Z. SDS-MoS2 Nanoparticles as Highly-efficient Peroxidase Mimetics for Colorimetric Detection of H2O2 and Glucose. *Talanta* **2015**, *141*, 47−52.
(50) Nirala, N. R.; Pandey, S.; Bansal, A.; Singh, V. K.; Mukherjee, B.; Saxena, P. S.; Srivastava, A. Different Shades of Cholesterol: Gold Nanoparticles Supported on MoS2 Nanoribbons for Enhanced Colorimetric Sensing of Free Cholesterol. *Biosens. Bioelectron.* **2015**, *74*, 207−213.
(51) Smith, R. J.; King, P. J.; Lotya, M.; Wirtz, C.; Khan, U.; De, S.; O'Neill, A.; Duesberg, G. S.; Grunlan, J. C.; Moriarty, G.; Chen, J.; Wang, J. Z.; Minett, A. I.; Nicolosi, V.; Coleman, J. N. Large-Scale Exfoliation of Inorganic Layered Compounds in Aqueous Surfactant Solutions. *Adv. Mater.* **2011**, *23*, 3944−3948.
(52) Nandwana, V.; Ryoo, S. R.; Kanthala, S.; McMahon, K. M.; Rink, J. S.; Li, Y.; Venkatraman, S. S.; Thaxton, C. S.; Dravid, V. P. High-Density Lipoprotein-like Magnetic Nanostructures (HDL-MNS): Theranostic Agents for Cardiovascular Disease. *Chem. Mater.* **2017**, *29*, 2276−2282.
(53) Najmaei, S.; Liu, Z.; Zhou, W.; Zou, X. L.; Shi, G.; Lei, S. D.; Yakobson, B. I.; Idrobo, J. C.; Ajayan, P. M.; Lou, J. Vapour Phase Growth and Grain Boundary Structure of Molybdenum Disulphide Atomic Layers. *Nat. Mater.* **2013**, *12*, 754−759.
(54) Wu, S. F.; Huang, C. M.; Aivazian, G.; Ross, J. S.; Cobden, D. H.; Xu, X. D. Vapor-Solid Growth of High Optical Quality MoS2Monolayers with Near-Unity Valley Polarization. *ACS Nano* **2013**, *7*, 2768−2772.
(55) Novoselov, K. S.; Jiang, D.; Schedin, F.; Booth, T. J.; Khotkevich, V. V.; Morozov, S. V.; Geim, A. K. Two-dimensional Atomic Crystals. *Proc. Natl. Acad. Sci. U. S. A.* **2005**, *102*, 10451−10453.
(56) Lin, Z.; Carvalho, B. R.; Kahn, E.; Lv, R. T.; Rao, R.; Terrones, H.; Pimenta, M. A.; Terrones, M. Defect Engineering of Two-Dimensional Transition Metal Dichalcogenides. *2D Mater.* **2016**, *3*, 022002.
(57) Addou, R.; Colombo, L.; Wallace, R. M. Surface Defects on Natural MoS2. *ACS Appl. Mater. Interfaces* **2015**, *7*, 11921−11929.
(58) Vancso, P.; Magda, G. Z.; Peto, J.; Noh, J. Y.; Kim, Y. S.; Hwang, C.; Biro, L. P.; Tapaszto, L. The Intrinsic Defect Structure of Exfoliated MoS2 Single Layers Revealed by Scanning Tunneling Microscopy. *Sci. Rep.* **2016**, *6*, 29726.
(59) Liu, T.; Wang, C.; Gu, X.; Gong, H.; Cheng, L.; Shi, X. Z.; Feng, L. Z.; Sun, B. Q.; Liu, Z. Drug Delivery with PEGylated MoS2 Nano-sheets for Combined Photothermal and Chemotherapy of Cancer. *Adv. Mater.* **2014**, *26*, 3433−3440.
(60) Presolski, S.; Pumera, M. Covalent Functionalization of MoS2. *Mater. Today* **2016**, *19*, 140−145.
(61) Wang, T. Y.; Zhu, R. Z.; Zhuo, J. Q.; Zhu, Z. W.; Shao, Y. H.; Li, M. X. Direct Detection of DNA below ppb Level Based on Thionin-Functionalized Layered MoS2 Electrochemical Sensors. *Anal. Chem.* **2014**, *86*, 12064−12069.
(62) Forster, A.; Gemming, S.; Seifert, G.; Tomanek, D. Chemical and Electronic Repair Mechanism of Defects in MoS2Monolayers. *ACS Nano* **2017**, *11*, 9989−9996.
(63) Wang, S. S.; Wang, X. C.; Warner, J. H. All Chemical Vapor Deposition Growth of MoS2:h-BN Vertical Van Der Waals Heterostructures. *ACS Nano* **2015**, *9*, 5246−5254.
(64) George, A. S.; Mutlu, Z.; Ionescu, R.; Wu, R. J.; Jeong, J. S.; Bay, H. H.; Chai, Y.; Mkhoyan, K. A.; Ozkan, M.; Ozkan, C. S. Wafer Scale Synthesis and High Resolution Structural Characterization of Atomically Thin MoS2 Layers. *Adv. Funct. Mater.* **2014**, *24*, 7461−7466.
(65) Li, H.; Zhang, Q.; Yap, C. C. R.; Tay, B. K.; Edwin, T. H. T.; Olivier, A.; Baillargeat, D. From Bulk to Monolayer MoS2: Evolution of Raman Scattering. *Adv. Funct. Mater.* **2012**, *22*, 1385−1390.
(66) Poulin, S.; Franca, R.; Moreau-Belanger, L.; Sacher, E. Confirmation of X-ray Photoelectron Spectroscopy Peak Attributions of Nanoparticulate Iron Oxides, Using Symmetric Peak Component Line Shapes. *J. Phys. Chem. C* **2010**, *114*, 10711−10718.
(67) Yamashita, T.; Hayes, P. Analysis of XPS Spectra of Fe2+ and Fe3+ ions in Oxide Materials. *Appl. Surf. Sci.* **2008**, *254*, 2441−2449.
(68) Wilson, D.; Langell, M. A. XPS Analysis of Oleylamine/Oleic Acid Capped Fe3O4 Nanoparticles as a Function of Temperature. *Appl. Surf. Sci.* **2014**, *303*, 6−13.
(69) McCreary, K. M.; Hanbicki, A. T.; Robinson, J. T.; Cobas, E.; Culbertson, J. C.; Friedman, A. L.; Jernigan, G. G.; Jonker, B. T. Large-Area Synthesis of Continuous and Uniform MoS2Monolayer Films on Graphene. *Adv. Funct. Mater.* **2014**, *24*, 6449−6454.
(70) Li, Y.; Cain, J. D.; Hanson, E. D.; Murthy, A. A.; Hao, S. Q.; Shi, F. Y.; Li, Q. Q.; Wolverton, C.; Chen, X. Q.; Dravid, V. P. Au@MoS2 Core-Shell Heterostructures with Strong Light-Matter Interactions. *Nano Lett.* **2016**, *16*, 7696−7702.
(71) Hamid, M.; Khalil-ur-Rehman. Potential Applications of Peroxidases. *Food Chem.* **2009**, *115*, 1177−1186.
(72) Oliver, N. S.; Toumazou, C.; Cass, A. E. G.; Johnston, D. G. Glucose Sensors: A Review of Current and Emerging Technology. *Diabetic Med.* **2009**, *26*, 197−210.
(73) Hosoda, H.; Takasaki, W.; Oe, T.; Tsukamoto, R.; Nambara, T. A Comparison of Chromogenic Substrates for Horseradish-Peroxidase as a Label in Steroid Enzyme-Immunoassay. *Chem. Pharm. Bull.* **1986**, *34*, 4177−4182.
(74) Park, S.; Boo, H.; Chung, T. D. Electrochemical Non-enzymatic Glucose Sensors. *Anal. Chim. Acta* **2006**, *556*, 46−57.
(75) Samanta, A.; Dhar, B. B.; Devi, R. N. Novel Porous Silica Encapsulated Au Nanoreactors as Peroxidase Mimic for One-Pot Glucose Detection. *New J. Chem.* **2012**, *36*, 2625−2629.
(76) Qin, F. X.; Jia, S. Y.; Wang, F. F.; Wu, S. H.; Song, J.; Liu, Y. Hemin@Metal-Organic Framework with Peroxidase-like Activity and Its Application to Glucose Detection. *Catal. Sci. Technol.* **2013**, *3*, 2761−2768.
(77) Creran, B.; Li, X. N.; Duncan, B.; Kim, C. S.; Moyano, D. F.; Rotello, V. M. Detection of Bacteria Using Inkjet-Printed Enzymatic Test Strips. *ACS Appl. Mater. Interfaces* **2014**, *6*, 19525−19530.
(78) Badugu, R.; Lakowicz, J. R.; Geddes, C. D. Noninvasive Continuous Monitoring of Physiological Glucose Using a Monosaccharide-Sensing Contact Lens. *Anal. Chem.* **2004**, *76*, 610−618.
(79) Soni, A.; Jha, S. K. A Paper Strip Based Non-Invasive Glucose Biosensor for Salivary Analysis. *Biosens. Bioelectron.* **2015**, *67*, 763−768.
(80) Sashikumar, R.; Kannan, R. Salivary Glucose Levels and Oral Candidal Carriage in Type II Diabetics. *Oral Surg Oral Med. O* **2010**, *109*, 706−711.
(81) Du, Y. Q.; Zhang, W. J.; Wang, M. L. Sensing of Salivary Glucose Using Nano-Structured Biosensors. *Biosensors* **2016**, *6*, 10.

DOI: 10.1021/acsanm.8b00429
ACS Appl. Nano Mater. XXXX, XXX, XXX−XXX